Available online at www.sciencedirect.com
SCIENCE DIRECT®
Advances in Water Resources 26 (2003) 17–31
Advances in Water Resources
www.elsevier.com/locate/advwatres

Theoretical analysis of the worthiness of Henry and Elder problems as benchmarks of density-dependent groundwater flow models

M.J. Simpson [a], T.P. Clement [a,b,*]

[a] Centre for Water Research, Department of Environmental Engineering, The University of Western Australia, Nedlands, 6907 Australia
[b] Department of Civil Engineering, Auburn University, Auburn, AL 36830, USA

Received 12 February 2002; received in revised form 18 June 2002; accepted 23 August 2002

Abstract

Computer models must be tested to ensure that the mathematical statements and solution schemes accurately represent the physical processes of interest. Because the availability of benchmark problems for testing density-dependent groundwater models is limited, one should be careful in using these problems appropriately. Details of a Galerkin finite-element model for the simulation of density-dependent, variably saturated flow processes are presented here. The model is tested using the Henry salt-water intrusion problem and Elder salt convection problem. The quality of these benchmark problems is then evaluated by solving the problems in the standard density-coupled mode and in a new density-uncoupled mode. The differences between the solutions indicate that the Henry salt-water intrusion problem has limited usefulness in benchmarking density-dependent flow models because the internal flow dynamics are largely determined by the boundary forcing. Alternatively, the Elder salt-convection problem is more suited to the model testing process because the flow patterns are completely determined by the internal balance of pressure and gravity forces.

Keywords: Groundwater-modeling; Density-dependent flow; Unsaturated flow; Contaminant transport

1. Introduction

Benchmarking the performance of a numerical code against standard analytical solutions is the necessary first step in testing the correctness of the numerical approximations. The next logical step in the benchmarking process is testing the code to either reflect a laboratory-scale experimental data set or a field-scale case study. Completing these two benchmarking steps for a density-dependent flow model is a difficult task because the availability of analytical solutions or standard laboratory/field data sets for the density-dependent flow problem is limited [31]. This contrasts with those problems involving linear solute transport and/or density invariant groundwater flow, for which there exists several well known analytical and laboratory solutions to the governing equations [1,17].

In the literature there has been much discussion concerning the philosophy of the model benchmarking processes. While it is not the purpose of this communication to enter into this philosophical discussion, the inherent problems with model verification should be acknowledged. Konikow and Bredeheoft [20] and Oreskes et al. [24] argue that verification and validation of numerical models of natural systems is impossible, as true natural systems are not closed and numerical results are always non-unique. While the importance of this argument should not be understated, the recognition of these philosophical issues should not detract from the need for accurate model development and testing, as the process of mathematical modeling is one of the useful options available for gaining insight into complex natural systems.

Konikow and Bredeheoft [21] suggested that a simple acknowledgement by the groundwater modeling community might circumvent some of the philosophical issues associated with model validation and verification.

* Corresponding author. Tel.: +1-334-844-6268; fax: +1-334-844-6290.
E-mail addresses: simpson@cwr.uwa.edu.au (M.J. Simpson), clement@eng.auburn.edu (T.P. Clement).

0309-1708/03/$ - see front matter
PII: S0309-1708(02)00085-4

They argued that the terms *validation* and *verification* should not be used in relation to model testing as these terms convey a false sense of accuracy to the general public. Furthermore, they stated that groundwater modelers should acknowledge the philosophical problems with the terms *validation* and *verification* and refrain from using them, and they suggest the term *history matching* as a substitute. We propose and use the term *benchmarking* as a way to describe and expand upon the meaning of history matching. By using the term *benchmarking*, we imply that the numerical algorithm can reproduce the prior history of a well-defined problem. The term benchmarking is also broader in scope than history matching and refers to model testing against standard problems that have been sufficiently tested and are widely accepted by model developers. An additional property of benchmark problems is that they are well understood and have been tested against analytical expressions and/or well-controlled field and laboratory studies, as well as against several numerical solutions in published intercode comparison studies.

A review of the benchmark problems available for testing density-dependent groundwater flow indicates that the Henry salt-water intrusion problem, for which an analytical solution exists, and the Elder salt convection problem, for which laboratory and numerical data are available, are the most popular ones. Note that while this study focuses upon the Henry salt-water intrusion problem and the Elder salt convection problem, there are several other problems that have been used in the literature to benchmark density-dependent groundwater flow codes. For example, the HYDROCOIN level 1, case 5 salt-dome problem [25] has also been frequently cited in the literature as a benchmarking problem e.g., [15,19,23]. More recently, several newer problems have been devised and proposed as benchmarking standards e.g., [18,31]. Although we restricted this analysis to the two most popular benchmark problems, the methodology developed here could be used to perform a similar analysis upon other benchmark problems.

The objective of this study is to provide a comprehensive assessment of the worthiness of the Henry and Elder problems by benchmarking a density-dependent groundwater flow model. Details of a density-dependent numerical model are provided, in part, to show the complexity of the governing relations and therefore illustrate the importance of ensuring a thorough benchmark process. Once developed, the numerical model is used to solve the common Henry salt-water intrusion problem and the Elder salt convection problem. The model is then used to resolve these benchmark problems in an uncoupled mode. Comparing the coupled and uncoupled results facilitates a novel way to separate the effects caused purely by density-dependent effects from those caused by the boundary conditions. By analyzing the results of these coupled and uncoupled solutions for the Henry and Elder problems, a qualitative assessment of the worthiness of each problem is accomplished.

2. Modeling density-dependent groundwater flow

2.1. Governing equations and constitutive relations

The equations governing the movement of a fluid through a variably saturated porous medium subject to variable density conditions can be derived from mass and momentum conservation principles [10,13]. For the present study, only two-dimensional (vertical) flow is considered. The governing equations are a set of two, coupled, non-linear partial differential equations written in terms of the fresh water pressure head as the dependent variable [2]:

$$\frac{\partial(\beta\theta)}{\partial t} + S_s\beta\frac{\theta}{\phi}\frac{\partial\psi}{\partial t} = \frac{\partial}{\partial x}\left(\beta K(\theta)\frac{\partial\psi}{\partial x}\right) + \frac{\partial}{\partial z}\left(\beta K(\theta)\frac{\partial\psi}{\partial z}\right) + \frac{\partial\left(\beta^2 K(\theta)\right)}{\partial z} \tag{1}$$

$$\theta\frac{\partial C}{\partial t} = \beta\frac{\partial}{\partial x}\left(D_x\theta\frac{\partial C}{\partial x}\right) + \beta\frac{\partial}{\partial z}\left(D_z\theta\frac{\partial C}{\partial z}\right) - V_x\theta\frac{\partial C}{\partial x} - V_z\theta\frac{\partial C}{\partial z} \tag{2}$$

where θ is the water content of the porous medium, β is the ratio of the fluid density to a reference freshwater density, K [LT^{-1}] is the hydraulic conductivity of the porous medium, ψ [L] is the freshwater pressure head of the fluid, S_s [L^{-1}] is the specific storage coefficient for the porous medium, ϕ is the porosity of the porous medium, C [ML^{-3}] is the concentration of the solute which contributes to the density variation, D_i [L^2T^{-1}] is the total dispersion coefficient in the ith Cartesian direction and V_i [LT^{-1}] is the fluid velocity in the ith Cartesian direction.

Eqs. (1) and (2) are coupled through the β term which represents the relative difference between the density of the fluid to a reference freshwater density:

$$\rho = \rho_0\beta = \rho_0\left(1 + \varepsilon\overline{C}\right) \tag{3}$$

where ρ [ML^{-3}] is the fluid density, ρ_0 [ML^{-3}] is the reference fresh water density, $\overline{C}$ is a dimensionless concentration $\overline{C} = C/C_{max}$, where C_{max} [ML^{-3}] is the concentration corresponding to the maximum fluid density, and ε is a dimensionless measure of the difference between the maximum density and freshwater density defined by

$$\varepsilon = \frac{\rho_{max} - \rho_0}{\rho_0} \tag{4}$$

Eq. (1) governs the movement of the fluid under variably saturated, density-dependent conditions. Eq. (2) represents the movement of the solute through the action of

dispersion and advective processes. In addition the equations are coupled through the fluid velocity, which may be calculated through the application of Darcy's law once Eq. (1) has been solved:

$$V_i = -\frac{K}{\theta}\left(\frac{\partial \psi}{\partial x_i} + g_i \beta\right) \tag{5}$$

where g_i is the vector indicating the direction of the action of gravitational forces.

Once the spatial distribution of velocity is known, then the coefficients of dispersion can be evaluated using the relations [10]:

$$\begin{aligned} D_x &= \alpha_L \frac{V_x^2}{\|V\|} + \alpha_T \frac{V_z^2}{\|V\|} + D_m \\ D_z &= \alpha_L \frac{V_z^2}{\|V\|} + \alpha_T \frac{V_x^2}{\|V\|} + D_m \end{aligned} \tag{6}$$

where α_L [L] and α_T [L] are the longitudinal and transverse dispersivities, respectively, $\|V\|$ [LT^{-1}] is magnitude of the fluid velocity and D_m [L^2T^{-1}] is the molecular diffusion coefficient for the solute within the porous medium.

Eqs. (1)–(6) are the governing equations for density-dependent flow in variably saturated porous media. The variably saturated form of the density-dependent flow equations is considered because it is the most comprehensive way to describe general density-dependent flow conditions. Although the benchmark problems considered in this paper are only concerned with fully saturated conditions, there are several practical problems that involve variably saturated flow phenomena. For example, Boufadel et al. [3] showed how variably saturated conditions could influence the groundwater flow beneath salt-lakes.

2.2. Numerical solution strategy

The solution of equations defined by the system (1)–(6) poses an interesting numerical challenge, particularly because the system is non-linear. Under fully saturated density-dependent flow conditions the non-linearity in the system arises from the presence of β in both the groundwater flow and solute transport equations. For the case of variably saturated density-dependent conditions, the governing equations are further complicated by the more complex non-linear relationships between the fluid pressure and moisture content, as well as the fluid pressure and the unsaturated hydraulic conductivity of the porous medium.

The numerical solution of the governing equations was sought using the Galerkin finite-element technique. The discretization of the spatial domain is achieved using linear triangular elements. The transient, variably saturated groundwater flow equation is approximated using a lumped, backward Euler time stepping scheme. The modified Picard procedure is incorporated to alleviate the non-linearity in the flow equation for unsaturated conditions [4,5]. Once the flow equation is solved, then the fluid velocity is evaluated using a method proposed by Yeh [36]. This method for the evaluation of fluid velocities ensures that the Darcy flux across each element boundary is continuous and therefore guarantees conservation of mass at each element interface [36]. Once the spatial variation of the fluid velocity is known, the dispersion coefficients in the solute transport equation can be calculated. The solute transport equation is then solved using a lumped Galerkin finite element formulation that incorporates the use of a time-weighting scheme.

While the equations resulting from the application of the Galerkin finite-element-method have been documented for simple variably saturated flow [16] as well as for fully saturated, density-dependent flow [10], there has been no clear documentation of the integrated element equations for variably saturated, density-dependent groundwater flow. Therefore, the details of the Galerkin element matrices derived for the variably saturated density-dependent groundwater flow equations are summarized in Appendix A for reference purposes. The matrix equations have been derived by analytically integrating the governing equations over linear triangular elements; therefore the algorithm has the advantage of avoiding the need for any numerical integration, and the entries in the stiffness matrix and force vector can be directly assembled with little effort. In addition, while implementing the Yeh [36] algorithm it should be recognized that the global stiffness matrix for the evaluation of the x and z components of the Darcy flux are identical. Furthermore, the entries in these flux matrices depend only upon the area of the elements, so significant computational savings can be made by assembling the flux matrix once only during the simulation.

The steps used in the numerical solution algorithm are summarized in Fig. 1. To solve a well posed problem, at the beginning of each time step the concentrations are assumed known and therefore the spatial distribution β is known. The distribution of β is used to solve the groundwater flow equation to yield the freshwater pressure head distribution. The fluid pressure and hydraulic conductivity are used to evaluate the fluid velocity, which then allows the evaluation of the dispersion coefficients. The fluid velocities and dispersion coefficients are introduced into the transport equation, which is linearized using the value of β from the previous coupling iteration. The concentrations at the new time step are obtained and used to update β, which is substituted back into the flow equation. This solution procedure is repeated iteratively until the maximum change in the fluid pressure (or solute concentration) falls below some specified tolerance. The linearized systems of equations generated by the procedure are solved using a banded LU factorization algorithm.

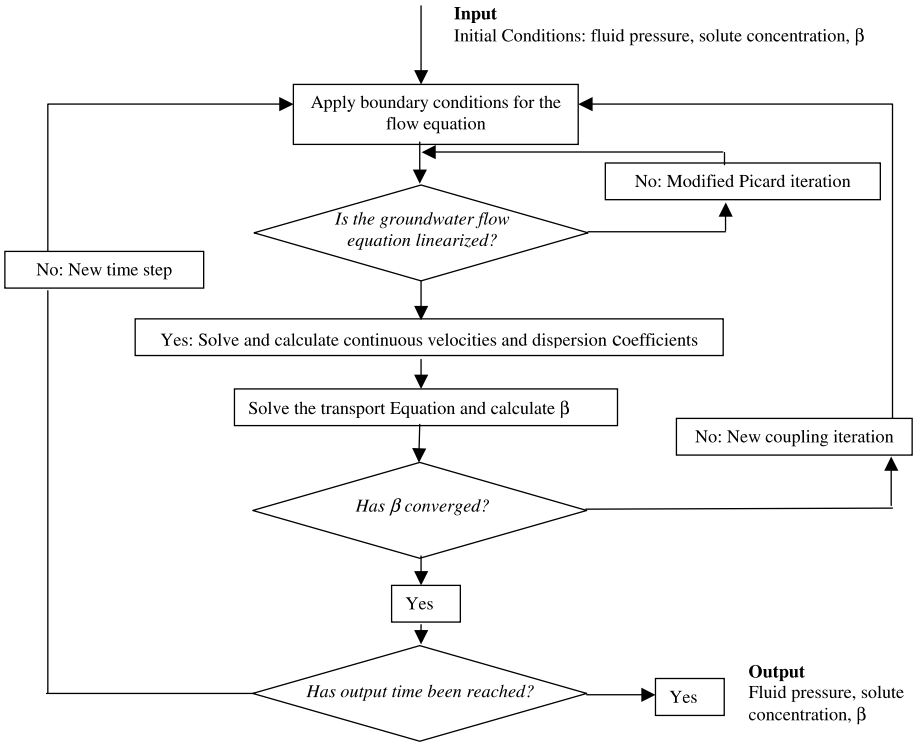

Fig. 1. Conceptual flow diagram showing the computational steps used to model density-dependent flow in variably saturated porous media.

3. Testing coupled groundwater flow and solute transport

Due to the complexity of the solution algorithm it is important to use benchmark problems to test whether the solution scheme is an accurate approximation of the partial differential equations. The relationships and coupling schemes are complex, therefore the only way to check the consistency is to use a previously benchmarked solution and compare it with the newly generated solution. To test the performance of the algorithm proposed in this study, two benchmark problems are solved and the results are compared against published solutions.

3.1. Henry's salt-water intrusion problem

In the literature, variable-density models are always benchmarked by solving the well-known Henry's salt-water intrusion problem [14]. Henry's problem is unique because an analytical solution exists; however, Henry's analytical solution is rather controversial. After almost 40 years of research, there has been a lot of discussion about the reproducibility and quality of Henry's original analytical solution [7,30]. Further complications have been introduced by the presentation of incorrect results; Voss and Souza [33] claimed that several analysts used an incorrect value for the total dispersion coefficient and that this trend was started by the work of Pinder and Cooper [26].

Several authors have also modified the original boundary conditions used by Henry to make the problem more realistic, this trend was started by Segol et al. [28]. The modified boundary condition involves making the original seaward boundary a combination of a partly freshwater and partly seawater boundary. While this may make the problem more realistic, the use of non-homogeneous boundary conditions precludes the use of Henry's analytical solution. Croucher and O'Sullivan [7] speculated that the original evaluation of Henry's analytical solution might have also been in error. Segol [30] re-evaluated the analytical solution and showed that the resulting governing equations differed in three places from those reported by Henry. Segol [30] then evaluated the revised analytical solution and demonstrated that it was in close agreement to a numerical solution of Henry's problem [30]. While this updated evaluation of Henry's analytical solution does correspond well with numerical solutions [30], it is the more realistic version of the Henry problem with the mixed seawater and freshwater boundary, as described by Frind [10] that is most frequently used as a benchmark problem. For example, several published models have used the solutions from Frind [10] to validate their density-dependent codes, e.g., [2,12,19]. Therefore, in this study, we used the modified Henry problem of Frind [10] as the standard benchmark problem.

The modified Henry's problem consists of a confined aquifer, which is subjected to a horizontal fresh-

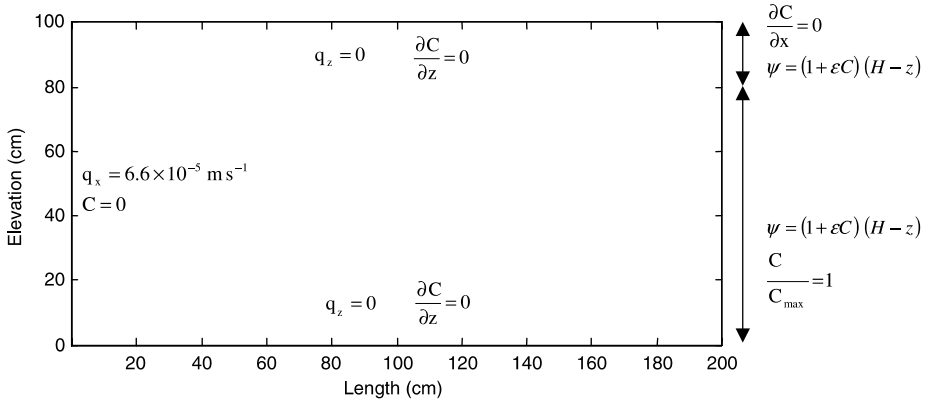

Fig. 2. Boundary conditions applied for solving the Henry salt-water intrusion problem.

Table 1
Aquifer properties used for the Henry problem [10]

Symbol	Quantity	Value	Unit
D_m	Coefficient of molecular diffusion	1.886×10^{-5}	$m^2\,s^{-1}$
g	Magnitude of gravitational acceleration	9.80	$m\,s^{-2}$
K	Hydraulic conductivity	1.0×10^{-2}	$m\,s^{-1}$
q	Recharge rate	6.6×10^{-5}	$m\,s^{-1}$
S_s	Specific storage	0.0	m^{-1}
β_{max}	Maximum density ratio	1.025	–
φ	Porosity	0.35	–
ρ_o	Reference density	1000	$kg\,m^{-3}$
ρ_{max}	Brine density	1025	$kg\,m^{-3}$

water recharge. The boundary conditions imposed on the aquifer are summarized in Fig. 2. The freshwater exits towards a sea boundary that is composed of a hydrostatic distribution of freshwater overlying heavier seawater. The model parameters used in the problem are shown in Table 1.

The simulation was performed upon a regularly discretized aquifer using 231 (21 horizontally, 11 vertically) nodes and 400 right-angled triangular elements. The initial condition for the problem was a quiescent aquifer composed of fresh water. The time step for the simulation was gradually increased by a factor of 1.2, starting at 12 s; the maximum time step allowed was 600 s. Temporal weighting of the transport equation was chosen such that a fully implicit solution was obtained. The iterative coupling scheme between the flow and transport equation was such that a minimum of two iterations was always performed, and then subsequent iterations were employed until the maximum change in the pressure head over any given time step was less than 0.005 m. This value of the coupling tolerance was selected because it was comparable to the coupling tolerance reported for a previously benchmarked code [33]. The model was run for 280 min, after which the density field did not change appreciably; this is consistent with other analysts who have obtained the steady solution within a similar time period [10]. Once the density field was stationary, the isochlor positions were obtained. Fig. 3 shows the 25%, 50% and 75% isochlors along with data points obtained from Frind [10]. The comparison of the 50% isochlor with that previously published shows that the present model is capable of reproducing the result observed by Frind [10].

In general, the Henry salt-water intrusion problem is usually numerically reproduced using a transient model

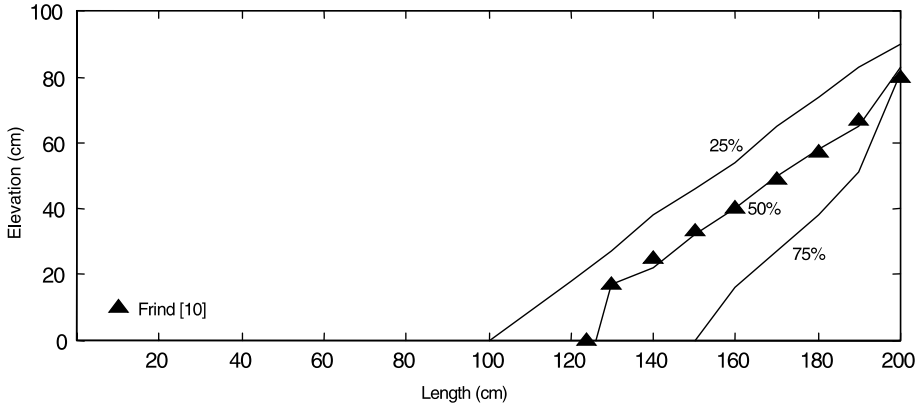

Fig. 3. Steady-state isochlor distribution for the Henry problem.

that is allowed to approach a steady profile over a long simulation period [2,10,12,19,28,33]. While the focus of the Henry salt-water intrusion problem is upon the generation of the steady-state profile, it is also possible to use the transient information to benchmark the model performance. However, care must be taken when using transient information since the results are sensitive to the initial condition used for the simulation. Normally, the initial condition for Henry's salt-water intrusion problem is a quiescent freshwater aquifer, although some analysts have started the simulation using the salt distribution predicted by the Ghyben-Herzberg hydrostatic assumption [10,26]. For the freshwater aquifer initial condition, it is possible to locate the position of the base of the 50% isochlor as it moves along the lower boundary of the aquifer. Frind [10] also solved the problem for the freshwater aquifer initial condition. The model data for the movement of the 50% isochlor provided by Frind [10] is compared against the present model results for the 25%, 50% and 75% isochlors in Fig. 4. Since the transient data are readily available from a density-dependent flow simulation, it is envisaged that this temporal data analysis should become a common task in the benchmarking process.

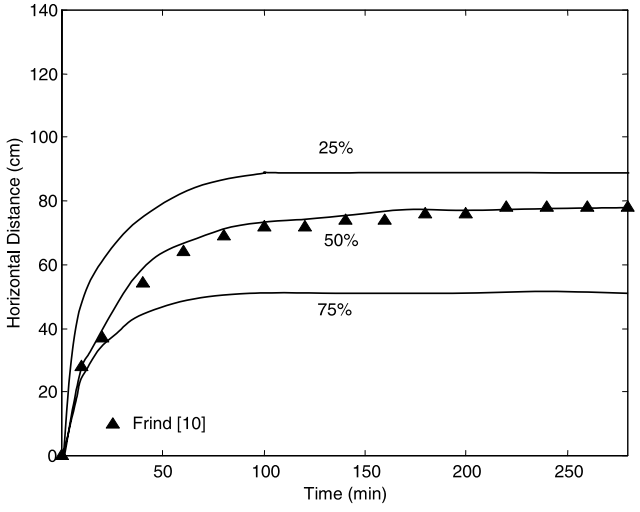

Fig. 4. Transient position of the toe of the saline water for the Henry problem.

3.2. The Elder salt convection problem

The original problem studied by Elder [8] concerned laminar fluid flow in a closed rectangular box modeled in cross-section. The flow within the box was initiated by a vertical temperature gradient, and thermally induced density gradients caused a complex pattern of fingering of the denser water to mix through the box. This problem was studied both physically in the laboratory with the use of a Hele-Shaw cell as well as being numerically reproduced. Since the laboratory conditions restricted the fluid flow to laminar conditions, Elder [9] also developed a modified problem with parameters suited to porous media flow where the density-dependence was caused by solute variations. This modified Elder problem is another standard benchmark problem used for testing several density-dependent flow codes [3,15,19,23], this problem shall be referred to herein as the Elder salt-convection problem. The maximum fluid density for the Elder salt convection problem is 1200 kg/m^3, hence the problem is often classified as a brine transport problem. Some of the difficulties in describing and predicting brine flows have been discussed by Hassanizadeh and Leijnse [13] and Watson and Barry [34].

The domain and boundary conditions for the Elder salt convection problem describe a closed aquifer, a zero pressure head is maintained on the two upper corners of the domain (Fig. 5). The aquifer properties and solute transport characteristics are summarized in Table 2. In our study the domain is regularly discretized using 3131 nodes (101 horizontally, 31 vertically) and 6000 right-angled linear triangular elements. The temporal discretization was maintained at a constant interval of one month, and the iterative coupling between the groundwater flow and solute transport equations was considered complete when the maximum change in the freshwater pressure head between iterations was smaller than 0.005 m [33]. A fully implicit temporal weighting

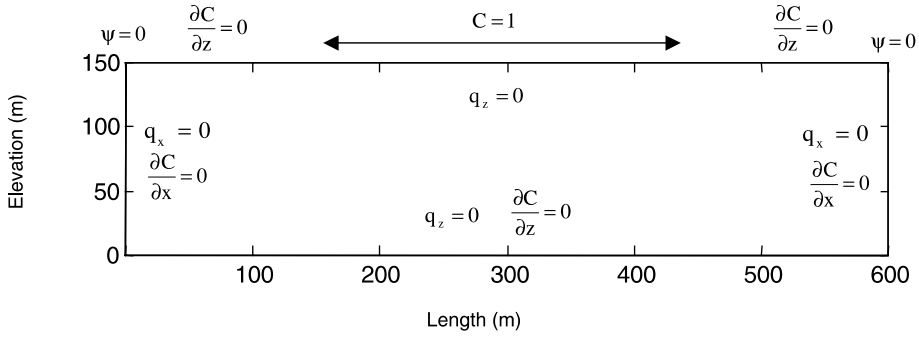

Fig. 5. Domain and boundary conditions for the Elder problem.

Table 2
Aquifer and transport properties used for the Elder problem [33]

Symbol	Quantity	Value	Unit
D_m	Coefficient of molecular diffusion	3.565×10^{-6}	$m^2\,s^{-1}$
g	Magnitude of gravitational acceleration	9.81	$m\,s^{-2}$
k	Intrinsic permeability	4.845×10^{-13}	m^2
β_{max}	Maximum density ratio	1.2	–
S_s	Specific storage	0.0	m^{-1}
φ	Porosity	0.1	–
μ	Dynamic viscosity	1×10^{-3}	$kg\,m^{-1}\,s^{-1}$
ρ_o	Reference density	1000	$kg\,m^{-3}$
ρ_{max}	Brine density	1200	$kg\,m^{-3}$

scheme was used to approximate the transport equation. The distribution of the coupled flow and transport characteristics was determined after 2, 4 and 10 years of simulation. The solute concentration profiles produced by the model show the generation of a series of transient vortices, which spread the solute throughout the aquifer through the action of both advection and molecular diffusion (Fig. 6). As expected, the distribution of the lobes of dense fluid is symmetric about the centerline of the aquifer.

Similar to the Henry problem, there are several published profiles available for the Elder salt convection problem. For example, previously published profiles by Voss and Souza [33] and Elder [9] are compared to the present profiles in Fig. 7. Comparing these profiles, one could draw two conclusions; firstly, the current model is capable of reproducing the solute concentration patterns reasonably well. Secondly, the comparison shows the

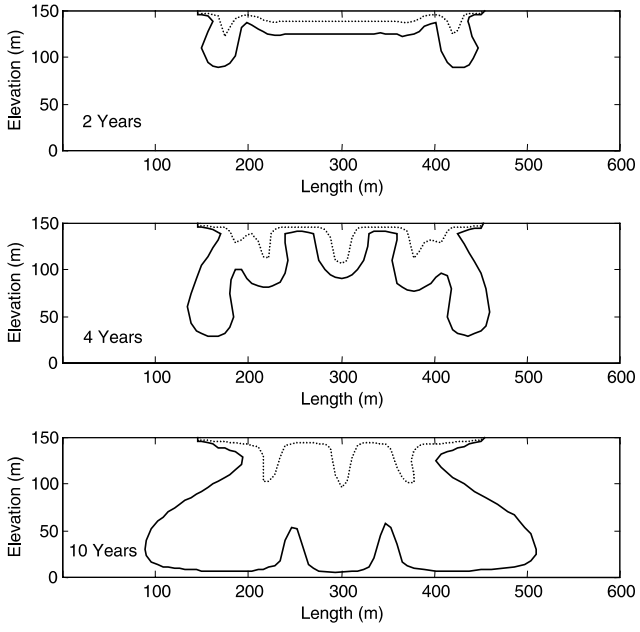

Fig. 6. Evolution of the flow pattern of the dense fluid into the aquifer for the Elder problem (20% isochlor solid, 60% isochlor dotted), showing the pattern after 2, 4 and 10 years.

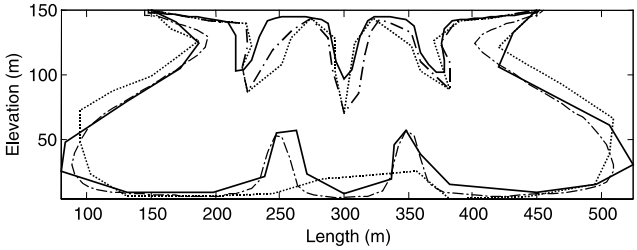

Fig. 7. Comparison of the 20% and 60% isochlors for the Elder problem after 10 years, by Elder [9] (—), Voss and Souza [33] (· · ·) and the present model (- · -).

difficulty in quantitatively benchmarking the Elder salt convection problem. Unfortunately, benchmarking the Elder results can be a tedious task as the solutions available in the literature can differ dramatically depending upon the numerical discretization and level of modeling sophistication used to generate the results. For example, Kolditz et al. [19] showed that the Elder salt convection profiles depend upon the level of modeling sophistication chosen for the numerical representation of the density-dependent flow and transport processes. Furthermore, their work incorporated a mesh-refinement procedure to show that the results can be quite sensitive to the level of discretization used in the numerical representation of the problem [19]. More recently, a locally adaptive grid technique was used in conjunction with a perturbation study to investigate the non-unique nature of the stationary solutions to the Elder problem [11].

Another point of interest with the Elder salt convection problem was shown by Boufadel et al. [3], where the problem was simulated using linear triangular finite elements. The results of Boufadel et al. [3] showed that the problem is sensitive to mesh-induced anisotropy when discretized with regularly aligned linear triangular elements and that the mesh had to be refined to overcome these problems. Therefore, given the range of solutions presented in the literature, at best the analyst can only show a qualitative comparison to demonstrate that the profiles generated by the new algorithm capture the essential features of the problem. This is why only a qualitative comparison between the profiles in Fig. 7 was possible for the benchmarking of the current numerical algorithm. In spite of this difficulty, the results from the present model captures the essential features of the fluid flow and the solute profiles are similar to those reported in the literature [3,19,23,33].

4. Evaluation of the worthiness of the modified Henry and Elder salt-convection problems

In order to assess the worthiness of both the Henry and Elder salt convection problems for the evaluation of the consistency of a density-dependent algorithm, the

problems were again solved after ignoring the coupling between the flow and transport equations. The basic objective of this task is to obtain a qualitative assessment of the degree to which the coupling is necessary to ensure that the problem of interest is solved correctly. If the coupled and uncoupled solutions are similar, then non-density-dependent processes must cause the interactions and therefore the problem is less worthy of being a benchmark problem. Alternatively, if there is a distinct difference between the coupled and uncoupled profiles then it is clear that the correct solution will only be obtained under the conditions where the numerical model accurately determines the balance of density-driven pressure and gravity forces.

4.1. Uncoupled Henry's salt-water intrusion problem

To investigate the solution of Henry's problem without coupling, β was fixed as unity for the solution of the fluid flow, fluid velocity and solute transport formulations. Other conditions in the numerical formulation were left the same. The simulation was performed for the same length of time, after which the uncoupled concentration field was stationary. The position of the 50% isochlor after this simulation was measured and compared with the coupled solution in Fig. 8. Comparing the position of the 50% isochlor for the coupled and uncoupled solutions shows that the profiles are quite similar. The reason for this similarity could be explained by comparing the coupled and uncoupled steady-state velocity profiles for the problem.

The steady-state velocity fields for the Henry saltwater intrusion problem for the coupled and uncoupled conditions are shown in Fig. 9. A comparison of the coupled and uncoupled velocity fields reveals some interesting results. The coupled velocity field shows that the horizontal velocities associated with the heavier saline water intrudes further into the aquifer than for the uncoupled solution. The region of interaction of the heavy saline fluid with the fresh recharged fluid is much broader under coupled conditions. For the coupled solution, the change in velocity in the lower area of the aquifer, where

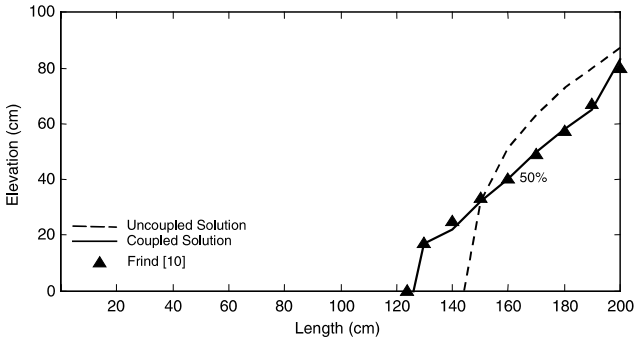

Fig. 8. Comparison of coupled and uncoupled solutions to the Henry problem.

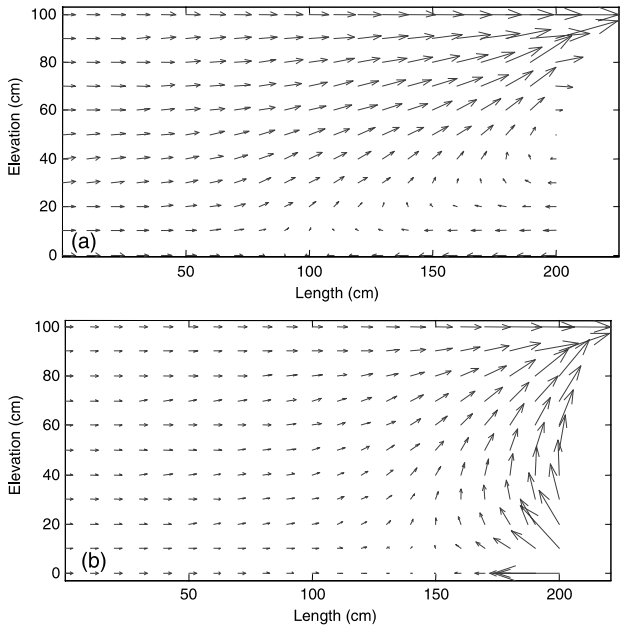

Fig. 9. Steady-state velocity field for the Henry problem under (a) coupled conditions and (b) uncoupled conditions.

the fresh and saline fluids interact, is quite sharp where as for the uncoupled solution the area of interaction is more gradual and smooth. This explains why the coupled 50% isochlor profile is not as smooth as the uncoupled 50% isochlor in Fig. 8. In general, the coupled and uncoupled flow patterns are largely the same. This similarity means that the density-dependent effects of the flow are not the key component in this test problem. In fact, the flow pattern in this problem is mostly determined by the imposed boundary conditions, which force the resulting distribution of pressures and concentrations.

It is also of interest to see whether this similarity between the coupled and uncoupled solution to Henry's saltwater intrusion problem is persistent for some simple variations of the basic problem. In order to investigate this, the original Henry problem was solved by increasing the value of the fresh water recharge rate to two times the original value and then again to four times the original recharge rate. The algorithm was run under these modified flow conditions in both coupled and uncoupled modes. In each case the algorithm was executed for 280 min, after this time the density field became steady (Fig. 10).

As the recharge into the aquifer increases, the equilibrium position of the intruded water is pushed back towards the sea boundary. Interestingly, the similarity between the coupled and uncoupled profiles increased as the recharge is increased. This serves to show that the similarity in the coupled and uncoupled solutions observed for the original case was not an isolated example. The Henry problem does suffer from the problem that the true profile is largely determined by the boundary forcing and much less by the density-dependent effects.

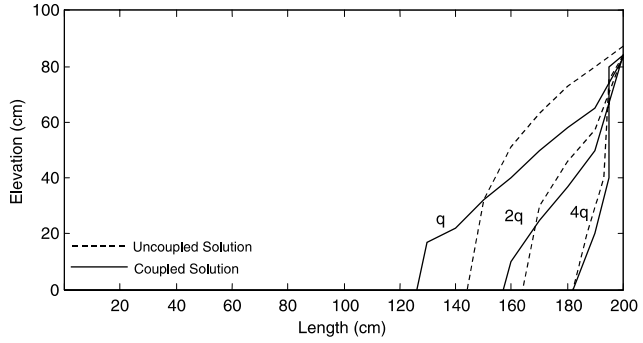

Fig. 10. Comparison of the coupled and uncoupled 50% isochlor profiles for varying recharge in the Henry problem.

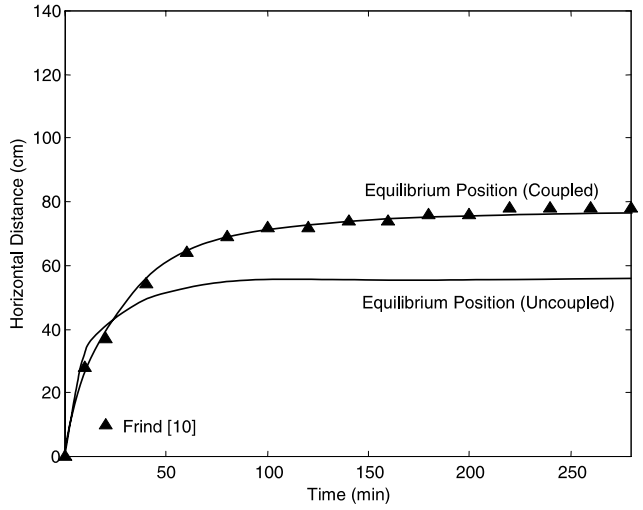

Fig. 11. Comparison of the transient position of the 50% isochlor moving along the base of the aquifer for the Henry problem.

It is also possible to obtain transient information regarding the solution to Henry's problem in the uncoupled mode. Fig. 11 shows the transient movement of the position of the uncoupled 50% isochlor for the Henry problem as it progresses along the base of the aquifer towards the steady position. The results from this observation show that there is a marked difference between the coupled and uncoupled profiles. Firstly, as observed in Fig. 8, the uncoupled isochlor does not advance as far into the aquifer as does the coupled isochlor; secondly, the uncoupled profile becomes steady well before the coupled solution. Therefore, it seems that the best methodology for the observation of the differences between the uncoupled and coupled solutions is in the analysis of this transient data.

4.2. Uncoupled Elder salt convection problem

The analysis of the uncoupled Elder salt convection problem is quite straightforward. Since the boundary conditions for the flow equation describes a closed aquifer, the only way that the solute can enter the aquifer is through pure molecular diffusion of the solute into the porous medium.

The simulation of the uncoupled profiles shows a simple diffusion pattern into the aquifer (Fig. 12). This is a rather obvious result; the simple diffusion pattern is expected because the fluid in the aquifer is stationary with a fixed concentration boundary along the upper surface. Since there is no feedback between the fluid concentration and the velocity, there is no advection under the uncoupled conditions. A comparison of the results shown in Figs. 6 and 12 clearly demonstrates that the correct solution to the Elder problem is completely dependent upon the accuracy of the coupling scheme. The symmetric lobes generated in the coupled solution are caused by the diffusion of the solute from the top boundary into the underlying fresh aquifer water. This then enters a feedback loop whereby the heavier saline water moves down faster than the surrounding waters. This causes advection of the solute into the aquifer and sets up the complicated convective fingering pattern. Once this occurs, then the spatial and temporal changes in β affect the groundwater flow equation and the entire system becomes strongly coupled. Analyzing the velocity field for the Elder salt-convection problem can show the importance of this coupling. Fig. 13 shows the coupled velocity field for the left-hand side of the aquifer after four years of simulation. While previous investigations have reported the velocity field for the Elder problem [3,33], re-iterating this diagram serves to show the significance of the problem as a benchmarking tool.

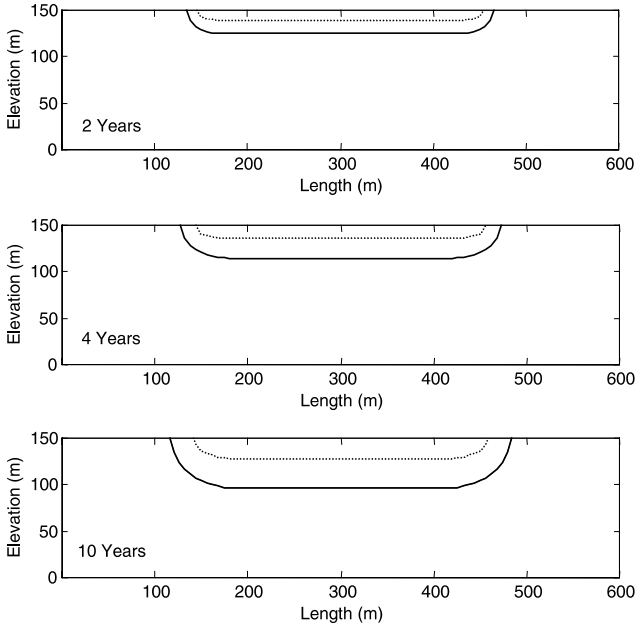

Fig. 12. Evolution of the solute profile into the aquifer for the uncoupled Elder salt convection problem (20% isochlor solid, 60% isochlor dashed) showing the pattern after 2, 4 and 10 years.

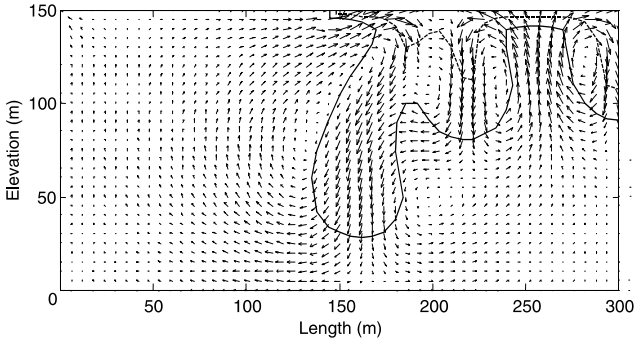

Fig. 13. The velocity field for the Elder problem after four years: 20% isochlor (—); 60% isochlor (- - -).

The distribution of the solute is dependent upon the velocity field; but the velocity field is also dependent upon the solute concentration and without the coupling between the flow and solute processes the fluid velocity within the aquifer would be zero.

Since the uncoupled Elder salt convection problem is a simple diffusion problem, we can use an analytical solution to check the predicted location of the advancing concentration front. Assuming one-dimensional conditions along the centerline of the front, the apparent length-scale of the advancing front can be computed using the following analytical solution [6]:

$$\frac{C}{C_0} = \operatorname{erfc}\left(\frac{z}{2\sqrt{Dt}}\right) \tag{7}$$

where C/C_0 is the relative concentration of the solute, z [L] is the length-scale traveled by the solute, and erfc is the complimentary error function. Table 3 compared the length-scales of the 20% and 60% relative concentrations, after 2, 4 and 10 years predicted using the analytical and numerical solutions. The numerical model length-scales were estimated from the results presented in Fig. 12. The Table shows a good correspondence between the analytical and numerical results.

A comparison of the coupled and uncoupled solutions to the Elder problem shows that the problem is indeed worthy of being used as a benchmark. This is because the problem can only be solved correctly when the numerical code encompasses all of the intricacies of the correct representations of the equations, their coupling, and the associated constitutive relationships.

Table 3
Comparison of length-scales of the diffusion front predicted by the uncoupled Elder solution and the analytical solution

Time (years)	Isochlor	Length—numerical (m)	Length—analytical (m)
2	20%	10	11
2	60%	26	27
4	20%	15	16
4	60%	37	38
10	20%	24	25
10	60%	58	60

5. Discussion

The results of this worthiness analysis have several implications for studies that attempt to benchmark a density-dependent groundwater model. Traditionally, the focus of benchmarking studies has been centered upon the Henry problem. In the past, several density-dependent groundwater models have been used to simulate field-scale problems after only being tested against the Henry problem. Segol and Pinder [29] simulated a real field-scale saltwater intrusion problem using the models developed by Pinder and Cooper [26] and Segol et al. [28] after benchmarking against the Henry problem only. Similarly, the work of both Frind [10] and Galeati et al. [12] developed density-dependent models that were tested against the Henry's problem alone and then immediately used to solve field-scale problems. Since the actual solution to Henry's problem is rather obscure due to the complications with the analytical solution as well as the publication of incorrect solutions, it is clear that care must be taken when comparing the new model results to those previously established. Given that the coupled solution in terms of the isochlor distribution looks very similar to the uncoupled solution, it is conceivable that an algorithm which does not correctly solve and couple the governing equations could generate a solution that might appear to be similar to the true solution.

These problems with the Henry salt-water intrusion problem have been further compounded by the way the results for the problem are commonly presented in the density-dependent flow modeling literature. Typically, in the solution of the Henry problem, the analyst presents the isochlor distribution alone [2,12,19]. While it is a necessary condition for the algorithm to be correct that the isochlors must be comparable to those from previous work, it may not be sufficient to claim that that the problem has been accurately solved simply because the isochlor positions are comparable.

Several points that can aid the benchmarking of a density-dependent model using the Henry problem have been raised in this discussion. Firstly, the velocity field should be used as a qualitative check of the correctness of the internal mixing environment within the aquifer before the solution is deemed adequate. Secondly, if the density-dependent model is used in a transient fashion to obtain the isochlor profiles, then it is important to locate the transient position of the intruded toe of the saline water and use this as an additional point of reference to benchmark the code. Finally, it is worthwhile to test the sensitivity of the model to the coupled and uncoupled conditions as demonstrated in this work.

There are some obvious fundamental differences between the Elder and the Henry problems. The most striking difference is that the Henry problem involves a stable density stratification where the denser fluid un-

derlies the lighter fluid, while the Elder problem involves an unstable density stratification where the heavier fluid overlies the lighter fresh water. In addition, a comparison of the Rayleigh number for the Henry and Elder problems further explains in part, the fundamental differences between the problems. The Rayleigh number is the ratio between the buoyancy-driven fluxes and those caused by dispersion processes. The Rayleigh number determines the onset of instability and unstable fingering is expected when the Rayleigh number exceeds some critical value [31]. Evaluating the Rayleigh number using a standard expression given by Simmons et al. [31] shows that the Elder problem has a Rayleigh number which is two orders of magnitude higher than that of the Henry problem. While the consequences of this difference is intuitive, it is not possible to assess whether this fundamental difference alone shall dictate the worthiness of the problem for benchmarking purposes.

The magnitude of the density differences observed in the Henry and Elder problems is another major difference between these two problems. The Henry salt-water intrusion problem deals only with seawater concentrations; therefore the maximum value of β in the flow and transport equations is 1.025. This contrasts with the Elder salt-convection problem where the maximum value of β is 1.2. The immediate effect of this difference is that the coupling between the equations is much stronger than for Henry's problem. This was observed during the numerical simulations for this study as the solution of the Henry problem required only two coupling iterations between the groundwater flow and transport equations, while the Elder salt convection problem required about four iterations. The additional iterations were required because, when solving the transport equation with the values of β from the previous iteration, there is likely to be some discrepancy between the concentration values predicted and the values of β used in the transport equation. This discrepancy was always more pronounced for the Elder problem, and explains why more coupling iterations were required than for the Henry problem. In fact, historically the Henry problem has been successfully solved using a single step updating scheme where there is no iteration between the groundwater flow and transport equations, instead the values are simply updated [2,10]. Because the larger value of ε (Eq. (4)) for the Elder salt-convection problem, a simple updating scheme is inadequate to provide sufficient coupling between the groundwater flow and solute transport equations. Therefore, the Elder salt convection problem has a greater worthiness as a benchmark problem as it is a thorough test for evaluating the integrity of the iterative coupling scheme used for the simulation of density-dependent groundwater flow.

Some limitations with the use of the Elder problem for benchmarking have also been identified. Due to the sensitivity of the Elder problem to numerical discretization and numerical representation there are several profiles in the literature, none of which are completely uniform. Therefore, at best the analyst can only use these profiles as a qualitative measure for the benchmarking process.

6. Summary and conclusions

The worthiness of both the Henry salt-water intrusion problem and the Elder salt convection problem were studied to assess their suitability to be used as benchmark problems for a density-dependent groundwater modeling code. Details of a Galerkin finite element numerical algorithm for solving density-dependent flow in variably saturated porous medium are provided. The mathematical model was tested and benchmarked by solving both the Henry and Elder salt convection problems and comparing the solutions against other published profiles. This testing procedure was able to show that the present model could reproduce established solutions of density-dependent groundwater flow problems. The tested model was then used to solve the problems in an uncoupled mode. A comparison of the coupled and uncoupled solutions provided a novel way to separate the density-dependent effects from other boundary effects that may impact the solution. The uncoupled solution of the Henry saltwater intrusion problem demonstrates that the patterns observed within the solution are insensitive to the density coupling of the equations. The solution from the uncoupled simulation looks similar to the correct solution. Therefore, the distribution of the saline water in Henry's problem is almost completely determined by the boundary forcing imposed on the problem, and not necessarily the result of density coupled flow and transport processes. Alternatively, the Elder salt convection problem has the advantage that the correct flow patterns are only achieved when the governing equations are correctly coupled. Therefore, the worthiness of the Elder problem as a benchmark standard is greater than that of the Henry problem.

In summary, both the Henry and Elder problems have their own advantages and disadvantages. The disadvantage of the Henry problem is that it is almost insensitive to density coupling effects, as illustrated in this study; however, the advantage is that the problem can be exactly reproduced to match previous results. On the other hand, the Elder problem is highly sensitive to density coupling effects, but the disadvantage of this problem is the results can be matched only in a qualitative sense because the problem is highly sensitive to discretization and other numerical convergence effects.

The results from this study indicate that a comparison of the coupled and uncoupled solutions to any standard density-dependant flow problem should always be

undertaken in order to assess the worthiness of the particular problem. Once the worthiness is established, then the benchmarking process can be focused upon those cases that show a large difference between the coupled and uncoupled solutions, such as the Elder problem, thereby ensuring the rigor of the benchmarking process.

Acknowledgements

We would like to acknowledge the comments from the Advances in Water Resources reviewers, in particular, Dr Craig Simmons. We would also like to thank Dr David Reynolds for his thorough review of the material. This work was made possible by the support provided by the Australian Postgraduate Award system through the Centre for Water Research and the University of Western Australia.

Appendix A. Finite element matrices

A.1. Flow equation

The solution to Eq. (1) is found by application of the Galerkin finite-element-method. Because the method has been discussed at length elsewhere only the most pertinent steps in the solution procedure are described to enable the reproduction of the algorithm. The dependent variable, ψ is approximated by a finite series of the form,

$$\psi(x,z,t) \approx \sum_{j=1}^{n} N_j(x,z)\widehat{\psi}(x,z,t) \tag{A.1}$$

The shape functions N_j, correspond to those associated with a linear triangular finite element interpolation scheme,

$$\widehat{\psi}(x,z,t) = \widehat{\psi}_i(t)N_i(x,z) + \widehat{\psi}_j(t)N_j(x,z) + \widehat{\psi}_k(t)N_k(x,z) \tag{A.2}$$

where,

$$N_r = \frac{1}{2A}[a_i + b_i x + c_i z] \quad N_s = \frac{1}{2A}[a_j + b_j x + c_j z]$$

$$N_t = \frac{1}{2A}[a_k + b_k x + c_k z]$$

$$a_i = x_j z_k - x_k z_j \quad b_i = z_j - z_k \quad c_i = x_k - x_j$$

$$a_j = x_k z_i - x_i z_k \quad b_j = z_k - z_i \quad c_j = x_i - x_k$$

$$a_k = x_i z_j - x_j z_i \quad b_k = z_i - z_j \quad c_k = x_j - x_i$$

where $\widehat{\psi}$ [L] is the interpolated freshwater pressure head, ψ_i, ψ_j and ψ_k [L] are the discrete values of the pressure head at the element vertices, N_i, N_j and N_k are the linear shape functions which depend upon the Cartesian coordinates (x,z) of the element vertices, and A [L^2] is the area of the element.

The basis of the Galerkin approach is that the trial solution shall form a residual when back substituted into the governing equation, the residual expression for the flow equation integrated over a particular element takes the form,

$$\begin{Bmatrix} R_i \\ R_j \\ R_k \end{Bmatrix} = \int_\Omega [N]^T \left[\frac{\partial}{\partial x}\left(\beta K(\theta)\frac{\partial \psi}{\partial x}\right) + \frac{\partial}{\partial z}\left(\beta K(\theta)\frac{\partial \psi}{\partial z}\right) + \frac{\partial(\beta^2 K(\theta))}{\partial z} - \frac{\partial(\beta\theta)}{\partial t} - S_s\beta\frac{\theta}{\eta}\frac{\partial \psi}{\partial t}\right] d\Omega \tag{A.3}$$

This integral is then split into five separate integrals corresponding each to the different terms in the equation. The shape functions correspond to those used for linear triangular elements, and then the integration is performed to yield the Galerkin matrices,

$$\begin{aligned}
\begin{Bmatrix} R_i \\ R_j \\ R_k \end{Bmatrix} &= -\frac{\left(\beta_i K_i^m + \beta_j K_j^m + \beta_k K_k^m\right)}{12A}\begin{bmatrix} b_i^2 & b_i b_j & b_i b_k \\ b_j b_i & b_j^2 & b_j b_k \\ b_k b_i & b_k b_j & b_k^2 \end{bmatrix} \\
&\times \begin{Bmatrix} \psi_i^{m+1,n+1} \\ \psi_j^{m+1,n+1} \\ \psi_k^{m+1,n+1} \end{Bmatrix} - \frac{\left(\beta_i K_i^m + \beta_j K_j^m + \beta_k K_k^m\right)}{12A} \\
&\times \begin{bmatrix} c_i^2 & c_i c_j & c_i c_k \\ c_j c_i & c_j^2 & c_j c_k \\ c_k c_i & c_k c_j & c_k^2 \end{bmatrix} \begin{Bmatrix} \psi_i^{m+1,n+1} \\ \psi_j^{m+1,n+1} \\ \psi_k^{m+1,n+1} \end{Bmatrix} \\
&+ \frac{1}{6}\begin{bmatrix} c_i\beta_i^2 K_i^m + c_j\beta_j^2 K_j^m + c_k\beta_k^2 K_k^m \\ c_i\beta_i^2 K_i^m + c_j\beta_j^2 K_j^m + c_k\beta_k^2 K_k^m \\ c_i\beta_i^2 K_i^m + c_j\beta_j^2 K_j^m + c_k\beta_k^2 K_k^m \end{bmatrix} \\
&- \frac{S_s}{3\phi\Delta t}\begin{bmatrix} \beta_i\theta_i^m & 0 & 0 \\ 0 & \beta_j\theta_j^m & 0 \\ 0 & 0 & \beta_k\theta_k^m \end{bmatrix} \begin{Bmatrix} \psi_i^{m+1,n+1} \\ \psi_j^{m+1,n+1} \\ \psi_k^{m+1,n+1} \end{Bmatrix} \\
&+ \frac{S_s}{3\phi\Delta t}\begin{bmatrix} \beta_i\theta_i^m & 0 & 0 \\ 0 & \beta_j\theta_j^m & 0 \\ 0 & 0 & \beta_k\theta_k^m \end{bmatrix} \begin{Bmatrix} \psi_i^n \\ \psi_j^n \\ \psi_k^n \end{Bmatrix} \\
&- \frac{A}{3\Delta t}\begin{bmatrix} \beta_i & 0 & 0 \\ 0 & \beta_j & 0 \\ 0 & 0 & \beta_k \end{bmatrix} \begin{Bmatrix} \theta_i^{m,n+1} - \theta_i^n \\ \theta_j^{m,n+1} - \theta_j^n \\ \theta_k^{m,n+1} - \theta_k^n \end{Bmatrix} \\
&- \frac{A}{3\Delta t}\begin{bmatrix} \beta_i \mathrm{Cap}_i^m & 0 & 0 \\ 0 & \beta_j \mathrm{Cap}_j^m & 0 \\ 0 & 0 & \beta_k \mathrm{Cap}_k^m \end{bmatrix} \begin{Bmatrix} \psi_i^{m+1,n+1} \\ \psi_j^{m+1,n+1} \\ \psi_k^{m+1,n+1} \end{Bmatrix} \\
&+ \frac{A}{3\Delta t}\begin{bmatrix} \beta_i \mathrm{Cap}_i^m & 0 & 0 \\ 0 & \beta_j \mathrm{Cap}_j^m & 0 \\ 0 & 0 & \beta_k \mathrm{Cap}_k^m \end{bmatrix} \begin{Bmatrix} \psi_i^{m,n+1} \\ \psi_j^{m,n+1} \\ \psi_k^{m,n+1} \end{Bmatrix} \\
&- \frac{A}{3\Delta t}\begin{bmatrix} \theta_i^m & 0 & 0 \\ 0 & \theta_j^m & 0 \\ 0 & 0 & \theta_k^m \end{bmatrix} \begin{Bmatrix} \beta_i^{n+1} - \beta_i^n \\ \beta_j^{n+1} - \beta_j^n \\ \beta_k^{n+1} - \beta_k^n \end{Bmatrix}
\end{aligned} \tag{A.4}$$

where the superscript $n+1$ refers to the value at the current time step while the superscript $m+1$ refers to the value of at the current Picard iteration step, and Cap

$[L^{-1}]$ is the slope of the retention function, all other terms have been previously defined.

The matrices in expression (A.4) which pre-multiply the column vectors of the unknown pressure heads contain the terms that form the global element stiffness matrix entries. The remaining vectors form the global element force vector. These expressions are evaluated individually and are assembled via the direct stiffness assembly procedure to form the global stiffness and global force vectors at each iteration within the algorithm. The application of Dirichlet and Neumann boundary conditions in the algorithm is straightforward, the methodology for implementing boundary conditions has been described elsewhere [27].

A.2. Velocity evaluation

The application of Darcy's law is made using the usual Galerkin approach to ensure that the fluid velocity is continuous over the entire domain, the residual expression for the vertical flux is,

$$\begin{Bmatrix} R_i \\ R_j \\ R_k \end{Bmatrix} = \int_\Omega [N]^T \left[q_z + K\frac{\partial \psi}{\partial z} - K\beta \right] d\Omega \tag{A.5}$$

Once (A.5) is integrated, the element matrices become,

$$\begin{Bmatrix} R_i \\ R_j \\ R_k \end{Bmatrix} = \frac{A}{24}\begin{bmatrix} 4 & 2 & 2 \\ 2 & 4 & 2 \\ 2 & 2 & 4 \end{bmatrix}\begin{Bmatrix} q_{zi} \\ q_{zj} \\ q_{zk} \end{Bmatrix} + \frac{(c_i\psi_i + c_j\psi_j + c_k\psi_k)}{24}\begin{Bmatrix} 2K_i + K_j + K_k \\ K_i + 2K_j + K_k \\ K_i + K_j + 2K_k \end{Bmatrix} + \frac{A}{24}\begin{Bmatrix} 4K_i\beta_i + 2K_j\beta_j + 2K_k\beta_k \\ 2K_i\beta_i + 4K_j\beta_j + 2K_k\beta_k \\ 2K_i\beta_i + 2K_j\beta_j + 4K_k\beta_k \end{Bmatrix} \tag{A.6}$$

The formulation for the horizontal flux is very similar, with the exception that there is no gravity term,

$$\begin{Bmatrix} R_i \\ R_j \\ R_k \end{Bmatrix} = \int_\Omega [N]^T \left[q_x + K\frac{\partial \psi}{\partial x} \right] d\Omega \tag{A.7}$$

The Galerkin residual expression for the horizontal flux is,

$$\begin{Bmatrix} R_i \\ R_j \\ R_k \end{Bmatrix} = \frac{A}{24}\begin{bmatrix} 4 & 2 & 2 \\ 2 & 4 & 2 \\ 2 & 2 & 4 \end{bmatrix}\begin{Bmatrix} q_{xi} \\ q_{xj} \\ q_{xk} \end{Bmatrix} + \frac{(b_i\psi_i + b_j\psi_j + b_k\psi_k)}{24} \times \begin{Bmatrix} 2K_i + K_j + K_k \\ K_i + 2K_j + K_k \\ K_i + K_j + 2K_k \end{Bmatrix} \tag{A.8}$$

Once the global force vector and global stiffness matrix are assembled and solved, the solution yields the nodal values of the fluid flux. Inspection of the formulations (A.6) and (A.8) reveal that the global stiffness matrices for the evaluation of the fluxes are identical and depend only upon the area of the elements. Therefore, the global stiffness matrix need only be assembled once at the beginning of the algorithm and not at each iteration step as required by both the groundwater flow and solute transport equation. The nodal values of fluid flux obtained are converted into the nodal value of fluid velocity by dividing the flux value by the nodal water content.

A.3. Transport equation

The solution to equation (2) is found by applying a temporal weighting scheme to the usual Galerkin finite-element solution procedure. The general expression for the residual is,

$$\begin{Bmatrix} R_i \\ R_j \\ R_k \end{Bmatrix} = \int_\Omega [N]^T \left[\beta\frac{\partial}{\partial x}\left(D_x\theta\frac{\partial C}{\partial x} \right) + \beta\frac{\partial}{\partial z}\left(D_z\theta\frac{\partial C}{\partial z} \right) - V_x\theta\frac{\partial C}{\partial x} - V_z\theta\frac{\partial C}{\partial z} - \theta\frac{\partial C}{\partial t} \right] d\Omega \tag{A.9}$$

Integrating the terms in (A.9) and introducing a time-weighting factor w, yields the element matrices,

$$\begin{Bmatrix} R_i \\ R_j \\ R_k \end{Bmatrix} = -\frac{A}{3\Delta t}\begin{bmatrix} \theta_i^{n+1} & 0 & 0 \\ 0 & \theta_j^{n+1} & 0 \\ 0 & 0 & \theta_k^{n+1} \end{bmatrix}\begin{Bmatrix} C_i^{n+1} \\ C_j^{n+1} \\ C_k^{n+1} \end{Bmatrix} + \frac{A}{3\Delta t}\begin{bmatrix} \theta_i^{n} & 0 & 0 \\ 0 & \theta_j^{n} & 0 \\ 0 & 0 & \theta_k^{n} \end{bmatrix}\begin{Bmatrix} C_i^{n} \\ C_j^{n} \\ C_k^{n} \end{Bmatrix} - \frac{(\beta\theta D_x)_{\text{ave}}^{n+1} w}{4A}\begin{bmatrix} b_i^2 & b_ib_j & b_ib_k \\ b_jb_i & b_j^2 & b_jb_k \\ b_kb_i & b_kb_j & b_k^2 \end{bmatrix}\begin{Bmatrix} C_i^{n+1} \\ C_j^{n+1} \\ C_k^{n+1} \end{Bmatrix} - \frac{(\beta\theta D_x)_{\text{ave}}^{n}(1-w)}{4A}\begin{bmatrix} b_i^2 & b_ib_j & b_ib_k \\ b_jb_i & b_j^2 & b_jb_k \\ b_kb_i & b_kb_j & b_k^2 \end{bmatrix}\begin{Bmatrix} C_i^{n} \\ C_j^{n} \\ C_k^{n} \end{Bmatrix} - \frac{(\beta\theta D_z)_{\text{ave}}^{n+1} w}{4A}\begin{bmatrix} c_i^2 & c_ic_j & c_ic_k \\ c_jc_i & c_j^2 & c_jc_k \\ c_kc_i & c_kc_j & c_k^2 \end{bmatrix}\begin{Bmatrix} C_i^{n+1} \\ C_j^{n+1} \\ C_k^{n+1} \end{Bmatrix} - \frac{(\beta\theta D_z)_{\text{ave}}^{n}(1-w)}{4A}\begin{bmatrix} c_i^2 & c_ic_j & c_ic_k \\ c_jc_i & c_j^2 & c_jc_k \\ c_kc_i & c_kc_j & c_k^2 \end{bmatrix}\begin{Bmatrix} C_i^{n} \\ C_j^{n} \\ C_k^{n} \end{Bmatrix} - \frac{(\theta V_x)_{\text{ave}}^{n+1} w}{6}\begin{bmatrix} b_i & b_j & b_k \\ b_i & b_j & b_k \\ b_i & b_j & b_k \end{bmatrix}\begin{Bmatrix} C_i^{n+1} \\ C_j^{n+1} \\ C_k^{n+1} \end{Bmatrix} - \frac{(\theta V_x)_{\text{ave}}^{n}(1-w)}{6}\begin{bmatrix} b_i & b_j & b_k \\ b_i & b_j & b_k \\ b_i & b_j & b_k \end{bmatrix}\begin{Bmatrix} C_i^{n} \\ C_j^{n} \\ C_k^{n} \end{Bmatrix}$$

$$-\frac{(\theta V_x)^{n+1}_{\text{ave}} w}{6}\begin{bmatrix} c_i & c_j & c_k \\ c_i & c_j & c_k \\ c_i & c_j & c_k \end{bmatrix}\begin{Bmatrix} C^{n+1}_i \\ C^{n+1}_j \\ C^{n+1}_k \end{Bmatrix} -\frac{(\theta V_x)^{n}_{\text{ave}} (1-w)}{6}\begin{bmatrix} c_i & c_j & c_k \\ c_i & c_j & c_k \\ c_i & c_j & c_k \end{bmatrix}\begin{Bmatrix} C^{n}_i \\ C^{n}_j \\ C^{n}_k \end{Bmatrix} \tag{A.10}$$

where the superscript $n+1$ refers to the unknown value at the current time step while the superscript n refers to the known value at the previous time step. Note that the subscript ave refers to that particular quantity arithmetically averaged across the element from the nodal values.

The time weighting factor w, is limited to values between zero and one. Using a time weighting factor of one gives a fully implicit solution while using a weighting factor of a half gives a Crank–Nicholson solution. Using a time-weighting factor of less than a half generally result in excessive oscillatory behavior of the solution [27].

A.4. Retention functions

The model element equations presented in this Appendix make reference to the variably saturated nature of the governing equations. To solve a variably saturated problem, the functional relationship between the pressure head and the water content as well as the relationship between the hydraulic conductivity and the pressure head must be known. The soil properties can be described using van Genucten's [32] soil-water-retention function and Mualem's [22] variably saturated hydraulic conductivity function. A detailed discussion about the parameters required in variably saturated flow models and their meaning can be found in Clement et al. [5] and Wise et al. [35].

A.5. Discussion of the fully saturated flow solution

Both the Henry salt-water intrusion problem and the Elder salt-convection problem solved in this work are fully saturated flow problems. Making the variably saturated formulation relax to simulate a fully saturated problem is quite simple because the hydraulic conductivity of the porous medium is no longer a function of the pressure head, and the water content of the porous medium becomes a constant. Under these conditions, the capacity (Cap) terms in the element equations relax to zero, the hydraulic conductivity terms become uncoupled from the pressure heads and the governing flow equation becomes linear. Therefore, solutions to fully saturated problems may be obtained without the need for the inner modified Picard iteration.

References

[1] Bear J. Hydraulics of groundwater. New York: McGraw-Hill; 1979.
[2] Boufadel MC, Suidan MT, Venosa AD. A numerical model for density-and-viscosity-dependent flows in two-dimensional variably saturated porous media. J Contamin Hydrol 1999;37:1–20.
[3] Boufadel MC, Suidan MT, Venosa AD. Numerical modeling of water flow below dry salt lakes: effect of capillarity and viscosity. J Hydrol 1999;221:55–74.
[4] Celia MA, Bouloutas ET, Zarba RL. A general mass-conservative numerical solution of the unsaturated flow equation. Water Resour Res 1990;26:1483–96.
[5] Clement TP, Wise WR, Molz FJ. A physically based, two-dimensional, finite-difference algorithm for modeling variably saturated flow. J Hydrol 1994;161:71–90.
[6] Crank J. Mathematics of diffusion. London: Oxford University Press; 1956.
[7] Croucher AE, O'Sullivan MJ. The Henry problem for saltwater intrusion. Water Resour Res 1995;31(7):1809–14.
[8] Elder JW. Steady free convection in a porous medium heated from below. J Fluid Mech 1967;27:29–50.
[9] Elder JW. Transient convection in a porous medium. J Fluid Mech 1967;27:609–23.
[10] Frind EO. Simulation of long-term transient density-dependent transport in groundwater. Adv Water Resour 1982;5:73–88.
[11] Frolkovič JP, Schepper HDe. Numerical modelling of convection dominated transport coupled with density driven flow in porous media. Adv Water Resour 2001;24:63–72.
[12] Galeati G, Gambolati G, Neumann SP. Coupled and partially coupled Eularian–Lagrangian model of freshwater–seawater mixing. Water Resour Res 1992;28:149–65.
[13] Hassanizadeh SM, Leijnse T. On the modeling of brine transport in porous media. Water Resour Res 1988;24:321–30.
[14] Henry HR. Effects of dispersion on salt encroachment in coastal aquifers, sea water in coastal aquifers. US Geological Survey Water Supply Paper 1613-C, 1964, 70–84.
[15] Herbert AW, Jackson CP, Lever DA. Coupled groundwater flow and solute transport with fluid density strongly dependent upon concentration. Water Resour Res 1988;24:1781–95.
[16] Huyakorn PS, Thomas SD, Thompson BM. Techniques for making finite elements competitive in modeling flow in variably saturated porous media. Water Resour Res 1984;30:1099–115.
[17] Javandel I, Doughty C, Tsang CF. Groundwater transport: handbook of mathematical models. Washington DC: Americal Geophysical Union; 1984.
[18] Johannsen K, Kinzelbach W, Oswald S, Wittum G. The saltpool benchmark problem-numerical simulation of saltwater upcoming in a porous medium. Adv Water Resour 2002;25:335–48.
[19] Kolditz O, Ratke R, Diersch H-JG, Zielke W. Coupled groundwater flow and transport: 1. Verification of variable density flow and transport models. Adv Water Resour 1998;21:27–46.
[20] Konikow LF, Bredeheoft JD. Ground-water models cannot be validated. Adv Water Resour 1992;15:75–83.
[21] Konikow LF, Bredeheoft JD. Ground-water models: validate or invalidate. Ground Water 1993;31:178–9.
[22] Mualem Y. A new model for predicting hydraulic conductivity of unsaturated porous media. Water Resour Res 1976;12:513–22.
[23] Oldenburg CM, Pruess K. Dispersive transport dynamics in a strongly coupled groundwater-brine flow system. Water Resour Res 1995;31:289–302.
[24] Oreskes N, Shrader-Frechette K, Belitz K. Verification, validation and confirmation of numerical models in the earth sciences. Science 1994;263:641–6.
[25] Organisation for Economic Co-operation and Development. The international HYDROCOIN project—level 1: code verification, report, Nuclear Energy Agency, Paris, 1988.

[26] Pinder Jr GF, Cooper HH. A numerical technique for calculating the transient position of the saltwater front. Water Resour Res 1970;6(3):875–82.
[27] Pinder GF, Gray WG. Finite element simulation in surface and subsurface hydrology. New Jersey: Academic Press; 1977.
[28] Segol G, Pinder GF, Gray WG. A Galerkin-finite element technique for calculating the transient position of the saltwater front. Water Resour Res 1975;11:343–7.
[29] Segol G, Pinder GF. Transient simulation of saltwater intrusion in southeastern Florida. Water Resour Res 1976;12:65–70.
[30] Segol G. Classic groundwater simulations: proving and improving numerical models. Englewood Cliffs, New Jersey: Prentice-Hall; 1994.
[31] Simmons CT, Narayan KA, Wooding RA. On a test case for density-dependent flow and solute transport models: the salt lake problem. Water Resour Res 1999;35:3607–20.
[32] Van Genuchten MTh. A closed form equation for predicting the hydraulic conductivity of unsaturated soils. Soil Sci Soc Am J 1980;44:892–8.
[33] Voss CI, Souza WR. Variable density flow and solute transport simulation of regional aquifers containing a narrow freshwater saltwater transition zone. Water Resour Res 1987;23:1851–66.
[34] Watson SJ, Barry DA. Numerical analysis of stable brine displacements for evaluation of density dependent flow theory. Phys Chem Earth (B) 2001;26:325–31.
[35] Wise WR, Clement TP, Molz FJ. Variably saturated modeling of transient drainage: Sensitivity of soil properties. J Hydrol 1994;161:91–108.
[36] Yeh G-T. On the computation of Darcian velocity and mass balance in the finite element modeling of groundwater flow. Water Resour Res 1981;17:1529–34.